Current Pulmonology Reports (2020) 9:131–142
https://doi.org/10.1007/s13665-020-00257-9

INVITED COMMENTARY

Pulmonary MRI: Applications and Use Cases

Raza Mushtaq[1] · Usha Jayagurunathan[1] · Hina Arif-Tiwari[1] · Kavitha Yaddanapudi[1]

Accepted: 5 October 2020 / Published online: 26 October 2020

Abstract

Purpose of Review Magnetic resonance imaging (MRI) has robust soft tissue characterization capability which was previously limited to evaluation of the mediastinum, cardiac, and chest wall imaging. MRI has now progressed from an experimental tool to complementary and alternate radiation free imaging modality for optimal identification and comprehensive evaluation of the lung parenchyma including structural, functional, and real-time imaging covering lung nodules/masses, infections, interstitial lung disease, airway diseases, and vascular and pleural abnormalities.

Recent Findings Recent use of fast imaging techniques and respiratory gating has overcome several of the previously reported MRI technical difficulties such as respiratory, cardiac and diaphragmatic motion, as well as susceptibility related to air tissue interface in the lungs.

Summary MRI is a viable tool to the imaging armamentarium for the identification and characterization of pulmonary parenchymal abnormalities, providing complementary diagnostic information to computed tomography (CT), improving the non-invasive diagnostic accuracy and problem-solving for indeterminate lesions.

Keywords Pulmonary MRI · Lung MRI · Pulmonary nodule · Diffusion pulmonary MRI

Introduction

Computed tomography (CT) is the workhorse of thoracic imaging and extensively used for pulmonary parenchymal, airway, and vascular disease. However, the major drawback is radiation and lack of soft tissue characterization even at times with contrast on board [1–4]. This is further exacerbated by the different practices among medical centers, particularly in terms for over-scanning in chest CT, which can result in increased effective and organ radiation dose [5]. Historically, pulmonary magnetic resonance imaging (MRI) has been sparsely utilized with limited role of pulmonary parenchyma due to numerous technical difficulties in the early developments [6, 7].

Tremendous improvements in MRI techniques including parallel imaging, ultrafast sequences, and respiratory and cardiac gating have made possible the routine use of MRI in clinical practice for the evaluation of pulmonary parenchymal abnormalities. In addition to being a viable alternative to ionizing imaging modality, MRI has several advantages such as its ability to provide structural and functional information due to inherent and exquisite soft tissue resolution. MRI can aid in tissue characterization as a non-invasive alternative to biopsy to help guide medical management [8, 9]. In this paper, we will discuss applications and use of MRI in pulmonary imaging.

Pulmonary MRI Technique

A combination of sequences with different weighting is used to identify specific tissue properties like the presence of fat (fat suppressed sequence), hemorrhage (fat suppressed), cellularity (diffusion), and flowing blood (steady-state). This allows for diagnosis, assessing treatment response/recurrence in malignant lesions, evaluating pulmonary thromboembolism and as a problem-solving tool in some indeterminate lesions [9, 10•]. Several questions regarding MRI chest technique are addressed.

Field Strength of Magnet

Higher field strength magnets, 3T, have been employed for chest imaging which provides the potential benefit of better

This article is part of the Topical Collection on *Pulmonary Radiology*

✉ Raza Mushtaq
rmushtaq@radiology.arizona.edu

[1] Department of Medical Imaging, University of Arizona College of Medicine, 1501 N Campbell Ave, Tucson, AZ 85724, USA

signal-to-noise ratio and improved temporal resolution. Imaging at higher field strength does come at a cost particularly increased artifacts associated with susceptibly and field heterogeneity [10•, 11]. Nevertheless, chest MRI for evaluation of pulmonary parenchyma can be reliably performed on 1.5T scanners with satisfactory image quality [10•, 12••].

MR Imaging Protocol

Based on a consensus from an expert panel, Biederer et al. proposed and recommended a lung MRI protocol. This includes T2-weighted images (T2WI) with and without fat saturation and inversion recovery techniques to identify infiltrates and nodules with high fluid content. A 3D gradient echo T1-weighted images (T1WI) fat suppressed pre- and post-contrast sequence to identify nodules/lesions with high T1WI signal and to evaluate the perfusion characteristics of malignant lesions [12••]. High-resolution pulmonary angiography with 3D gradient echo T1WI sequence along with first pass perfusion for evaluation of pulmonary embolism and arteriovenous malformations. In patients with poor renal function, balanced steady-state free precision can be used to evaluate the pulmonary vasculature instead of administering contrast (Fig. 1) [13].

Evolving Role of Diffusion-Weighted Imaging

Diffusion-weighted imaging (DWI) was initially used in neuroradiology for stroke imaging, but its applications have broadened since its advent in body imaging as it requires no contrast and can be obtained with multiple and single breath hold [14, 15]. DWI technique investigates diffusion of water molecules within tissues [10•, 15]. This has a wide variety of application in body imaging.

In our practice, we have used DWI has a screening tool to identify and characterize lesions. Current studies are investigating the role of DWI in differentiating benign from malignant lesions with variable results [16]. In a meta-analysis of DWI for the differential diagnosis of lung lesions, Chen et al. concluded that DWI is a non-invasive, accurate technique for distinguishing benign from malignant lung lesions but requires further large-scale studies for standardization of the technique and cut off values [17•]. Further utility of DWI in the evaluation of treatment response and recurrent tumor in the lung is also being explored [15, 16]. The feasibility of DWI in detecting pulmonary embolism (PE) has been studied and has been shown to have high sensitivity but currently lacks specificity [18].

Fig. 1 Coronal MIP (maximum intensity projection) image of normal pulmonary arterial vasculature, similar to conventional angiography

Challenges in Thoracic MRI

Several limitations have been described in the literature preventing widespread utilization of thoracic MRI. Air-filled lungs pose a great challenge in pulmonary MRI due to local field heterogeneities resulting in susceptibility MRI artifacts; however, newer techniques relying on ultrafast echo time can overcome this hindrance [10•]. Currently, we can evaluate interstitial abnormalities with great detail allowing for accurate parenchymal diagnoses. Air-filled lungs are devoid of protons resulting in inherent lack of signal, previously thought to be a drawback, which has been found to be advantageous when evaluating space occupying lesions such as neoplasms or pneumonia that result in increased number or protons on T2WI [8, 10•].

Respiratory and cardiac motion has been a cited as a major shortcoming in interpreting thoracic MRI. While breath hold images can help overcome these issues, it is not feasible to use such techniques in chronically and critically ill patients. Respiratory and cardiac gating techniques along several other acquisition approaches have now overcome this limitation [10•, 19, 20]. Motion-resistant fluid sensitive sequences, such as T1-weighted imaging with and without fat saturation and steady-state free precision sequences, provide valuable information in those instances.

Lung Function Analysis

To evaluate lung function, pulmonary MRI using hyperpolarized inert gases have been studied. This is emerging as a clinical tool for the regional assessment of pulmonary function as opposed to global evaluation with spirometry and plethysmography. This is particularly helpful in early stages when the pulmonary abnormalities are regional and not evident on conventional testing [21].

Initial research used helium (He 3+) gas; however, with reduced availability and higher cost, it is now being replaced by xenon (Xe 129) gas. Other gases have also been explored including hyperpolarized oxygen (100% pure oxygen) and perfluorinated gases (sulfur hexafluoride, hexafluoroethane, perfluoropropane). Hyperpolarization of gases increases their

magnetization so that the gases can be used as contrast agents to image the airways and airspaces by increasing the T1 signal and decreasing the susceptibility effects [21, 22].

Subjects inhale about 0.5–1 L of hyperpolarized gas, and images are acquired in a single breath hold for ventilation-weighted and diffusion-weighted imaging. Ventilation maps shows areas with decreased ventilation as lacking enhancement which can be used to calculate the ventilation defect percentage (VDP)—defined as non-ventilated lung volume normalized to normal lung volume. Ebner and colleagues proposed the semiautomated linear binning model as a more objective way to quantify ventilation defects to reduce the operator dependence and increase reproducibility [21]. They rescaled the MR images to the 99th percentile of the cumulative distribution and used fixed thresholds to classify Xe voxels—defect, low, medium, and high intensities. The areas of defects and low signal intensity were used to calculate the ventilation defect percentage in patients with airway disorders such as COPD and asthma.

Xenon gas, similar to oxygen, dissolves in capillary membranes and binds to RBC, a property that has led to utilization of Xe as a surrogate marker for gas exchange, as identified on CSI and spectroscopy. By measuring the relative ratios of the spectral signal peaks in the alveolar gas, alveolocapillary membrane (barrier tissue), and RBC, semiquantitative assessment of gaseous exchange can be made which correlates well with diffusion capacity of carbon monoxide (DLCO) [21].

Any pathologic process that increases the thickness of the barrier tissue like pulmonary edema, inflammation, scarring, lymphangitic spread of malignancy, idiopathic pulmonary fibrosis results in a decrease in the free diffusion of gas molecules across the barrier tissue impairing gas exchange. In conclusion, pulmonary MRI with hyperpolarized gases would serve as a valuable tool in the long-term management of pulmonary disorders by combining ventilation images and gas exchange maps and currently is the only modality able to assess regional lung function.

Clinical Applications

MR Imaging of Pulmonary Parenchyma

Pulmonary Nodules

Pulmonary nodule is a well-defined opacity measuring up to 3 cm [23]. Increased utilization of CT in routine medical management has resulted in increased identification of incidental pulmonary nodules. A recent study of 2479 CT coronary angiograms found incidental nodules in 13.9% of the patients requiring follow-up imaging with high associated cost to medical care and cumulative radiation dose [24].

The primary clinical and radiological objective is to identify benign from malignant nodules. The Fleischner Society, a multidisciplinary international group, provides guidelines for management of incidental pulmonary nodules to reduce unnecessary follow-up examinations while capturing and managing high-risk patients [25]. CT remains the primary recommendation for evaluation of such nodules, as per ACR Appropriateness Criteria [26]. Current Fleischner guidelines recommend follow-up imaging for nodules greater than the size of 6 mm and follow-up for more invasive measures in patients with nodules greater than 8 mm depending on nodule characteristics and patient risk factors [25]. MRI has been shown to have 80% sensitivity in detection of a 4-mm nodule which increases quite significantly for nodules larger than 8 mm [12••]. A study of 113 pulmonary nodules with size greater than 4 mm assessed MRI detection rate and accuracy of size estimation as compared with CT. They found overall sensitivity of 80.5% with a strong agreement between size measurements between CT and MRI findings [27•]. Given these size requirements, MRI can be utilized for evaluation of pulmonary nodules with reduction in invasive measures and cumulative radiation from repeated CT studies. It is important to note that population studies that resulted in current guidelines were performed with CT and data for MRI in large population studies is currently lacking.

The superior contrast between nodules and the adjacent pulmonary parenchyma on CT allows for higher detection rate of the nodules; however, further characterization of the nodules can be difficult in absence of obvious malignant features such as spiculated margins or local invasion. MRI can aid in nodule characterization. Malignant nodules demonstrate low or intermediate signal on T1WI and slightly high signal on T2WI (Fig. 2). In a study of 49 patients with average nodule size of 15 mm, authors reported 78% sensitivity for detection of malignant pulmonary nodules using T2WI [28]. A pilot study evaluating feasibility of MRI for lung cancer screening by Meier-Schroers et al. concluded that malignant nodules, greater than 6 mm, have distinctive characteristics on MRI [29]. Studies utilizing machine learning have also found high sensitivity and accuracy in classification of pulmonary lesions using multiparametric MR sequences [30].

Perfusion characteristics of solitary pulmonary nodules have been investigated; several studies have shown early rapid enhancement in malignant and active inflammation correlating with rapid washout in malignant lesions [31]. Higher signal on T2WI can help distinguish malignant from surrounding inflammation. DWI has also been applied in attempt to differentiate benign from malignant pulmonary nodules with malignant nodules displaying a greater propensity to restrict diffusion as compared with benign nodules [31].

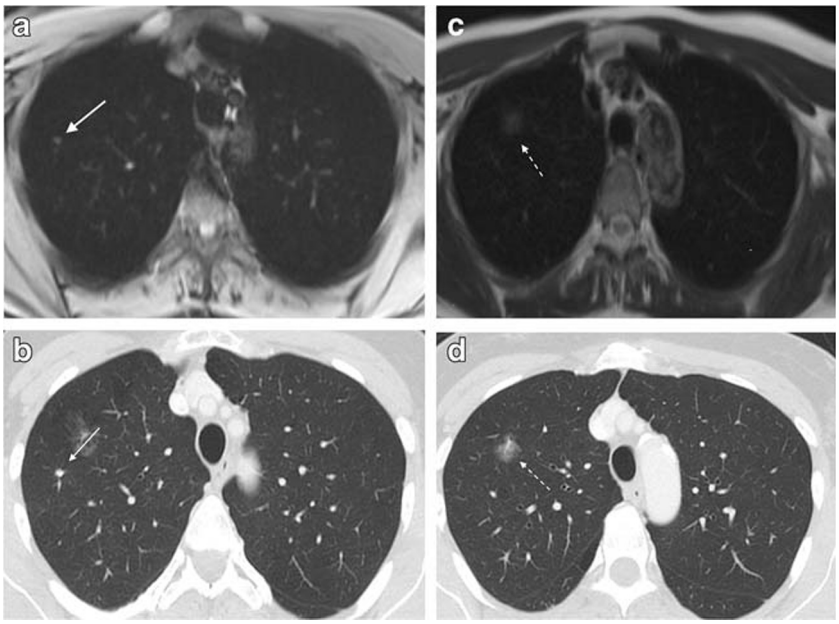

Fig. 2 Small nodules and adenocarcinoma. **a** Axial T1-weighted gradient echo image. **b** Corresponding axial CT shows a small 4 mm nodule in the right upper lobe (white arrow). **c** and **d** Axial T2- weighted image (**c**) with corresponding axial CT image (**d**) at the same level shows a groundglass nodule which was found to be an adenocarcinoma

Bronchogenic Carcinoma

Lung cancer remains the most common cause of cancer-related deaths in the western world despite new treatment options. CT and fluorine-18-fluoro-2-deoxy-d-glucose positron emission tomography (FDG-PET) are currently the imaging modality of choice in workup with limited role of MRI [32].

On MRI, primary lung tumors appear iso- to hypointense on T1WI and slightly hyperintense on T2WI (Figs. 3 and 4). Heterogenous signal intensity of the primary lesion may be due to varying degrees of necrosis appearing as hyperintense on T2WI and hemorrhage appearing as hyperintense signal on T1WI. Diffusion restriction on DWI is useful in differentiating centrally located neoplasms causing bronchial obstruction with obstructive atelectasis/consolidation from mucus plugging.

A subset of bronchogenic carcinoma arising from the superior sulcus was originally described by Pancoast [33, 34]. MRI has become an integral part of assessing superior sulcus tumor by providing superior soft tissue contrast evaluation of involvement of the adjacent chest well and neurovascular structures especially the brachial plexus [34]. A study of 31 patients undergoing superior sulcus tumor resection showed 94% accuracy of MRI, as compared with 63% of CT, in assessing local tumor invasion [35].

Metastases

Pulmonary metastases may present as solitary or multiple nodules and masses. Currently, MRI is not routinely used for pulmonary metastasis workup [36]. Comprehensive tumor staging is performed using MR imaging of the chest, abdomen, and pelvis for certain malignancies including those of gynecological, colorectal and pancreaticobiliary origin as a one stop investigation in our practice. Detection rate and sensitivity for metastases are the same as for nodules as described above.

MRI may be particularly useful in identifying melanoma metastases due to high signal on T1WI to the paramagnetic effects of melanin. The differential consideration would include hemorrhagic metastases as renal metastases.

Atelectasis

Collapse of lung is termed atelectasis which can be further classified based on etiology. Round atelectasis is the form of peripheral lung collapse adjacent to the pleura develops during the healing phase of pleural effusion and can be mistaken for a mass or infectious consolidation. Both CT and FDG-PET imaging cannot reliably differentiate malignancy from round atelectasis [37, 38]. MRI can be an invaluable tool by circumventing need for a biopsy. On T2WI and post-contrast images, the in-folded visceral pleura in round atelectasis is seen as a curvilinear hypointense line at the pleural aspect and curving bronchovascular structures along the pulmonary aspect. Non-obstructive atelectasis has low signal on T2W images whereas obstructive atelectasis has slightly elevated signal due to the accumulation of fluid within the obstructed airspace. Dynamic contrast imaging and DWI can further differentiate secretions from tumoral causes of obstruction [39, 40].

Pneumonia

Chest radiographs are considered the first line for evaluation of acute respiratory illness and pneumonia in immunocompetent and immunocompromised patients [41, 42]. However, MRI is more accurate than chest radiographs in detecting pneumonia and has similar efficacy as CT [42]. MRI can play an integral

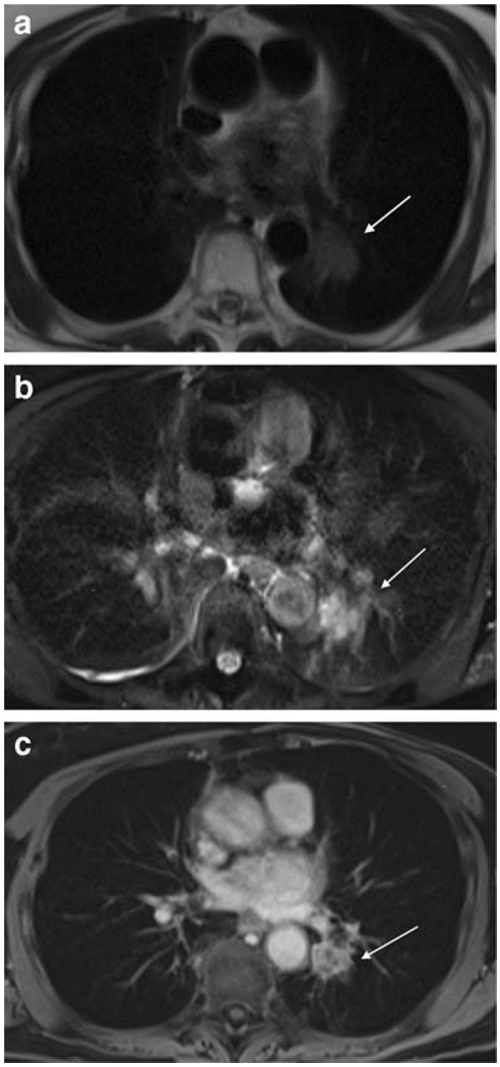

Fig. 3 Biopsy proven non-small cell lung cancer. **a** Axial T2-weighted without and **b** with fat saturation show a spiculated soft tissue mass in the superior segment of the left lower lobe. Notice how the spiculations are well identified on MRI similar to CT. There is avid but heterogenous enhancement on axial T1-weighted gradient echo image (**c**)

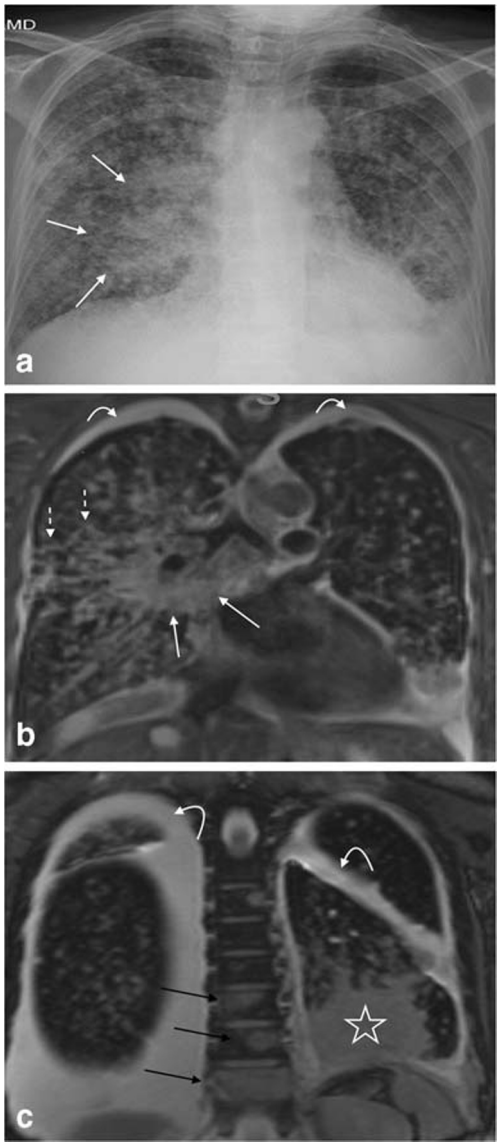

Fig. 4 New diagnosis of stage IV right hilar small cell lung cancer with lymphangitic spread and metastases. **a** Frontal chest radiograph shows a mass in the right hilar and infrahilar regions (white arrow). Further characterization with **b**, **c** coronal steady-state free precision images demonstrates a hyperintense right hilar mass contiguous with subcarinal lymphadenopathy (white arrows) which encases the bronchovascular structures in the hilum. There is lymphangitic spread as evidenced by nodular thickening of the peribronchovascular interstitium (white dashed arrows). Bilateral pleural effusions (curved arrows) and osseous axial osseous metastases (black arrows) were readily identified. Incidentally noted is compressive atelectasis of left lower lobe (star)

and complementary role in pneumonia in assessing complications, particularly in children and pregnant patients to avoid ionizing radiation [8, 43]. Infectious and inflammatory consolidations related to pneumonia appear bright on T2WI and enhance homogenously on post-contrast imaging. Complications such as necrosis and abscess formation (Figs. 5 and 6) can be readily ascertained on multiple MRI sequences [43]. Necrotizing pneumonia (Fig. 7) appears as internal cystic area with high signal on T2WI which lacks enhancement on post-contrast imaging. Empyema presents as a loculated area of pleural effusion with diffusion restriction and thick-walled enhancement [8].

Variant forms of pneumonia such as exogenous lipoid pneumonia, typically caused by inhalation or aspiration of fatty substances, can have non-specific CT features while it can be correctly characterized by MRI. Fat saturation techniques can help identify presence of fat within the consolidation [44].

Allergic bronchopulmonary aspergillosis (ABPA) is a pulmonary fungal infection resulting as a hypersensitivity reaction after colonization of bronchopulmonary structures with Aspergillus especially in patients with underlying disorders such as asthma and cystic fibrosis [45]. Currently, CT is utilized as the imaging modality of choice for ABPA evaluation [46, 47]. A recent prospective study of 27 patients evaluating diagnostic performance of MRI in diagnosis ABPA, using CT

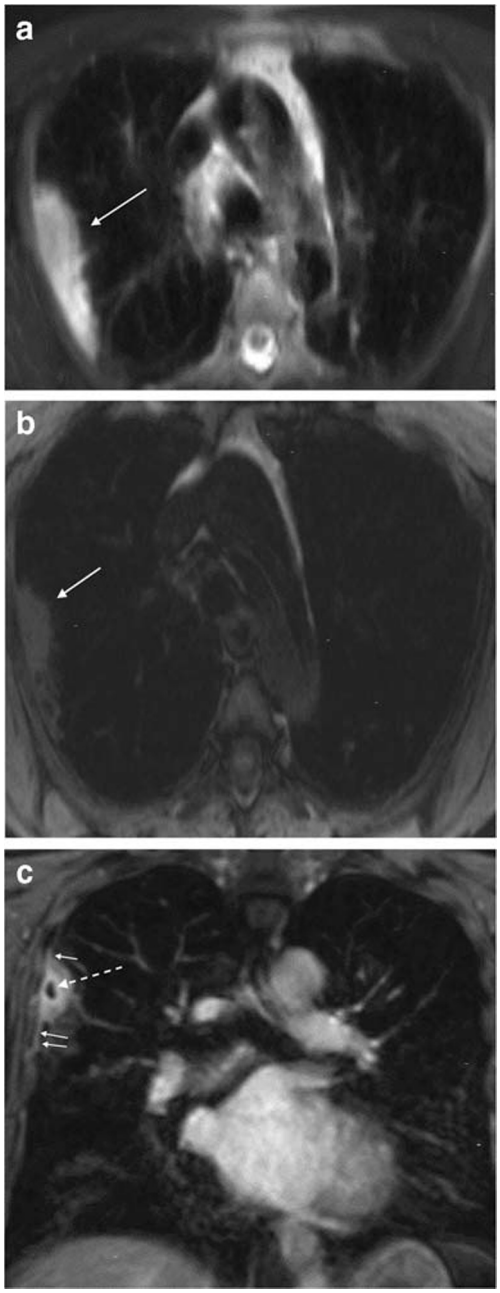

Fig. 5 Cocci necrotic pneumonia. **a** Axial fat–saturated T2-weighted image and **b** pre-contrast axial T1-weighted gradient echo image demonstrates a T2 hyperintense and T1 hypointense consolidation. **c** Coronal post-contrast T1-weighted gradient echo image shows avid enhancement with internal cavitation related to necrosis (dashed arrow) and associated pleural inflammation (short white arrows) positive for cocci on biopsy

findings as the reference standard, found high specify but low sensitivity (68%) in evaluating ABPA [47].

Tuberculoma

Pulmonary tuberculosis has a variety of imaging manifestations including consolidation, cavitary lesions, tree in bud

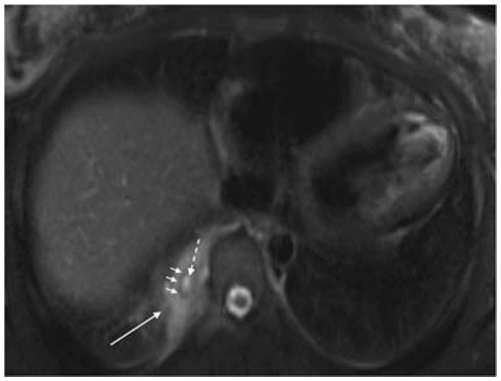

Fig. 6 Young female with history of intravenous drug abuse presenting for pulmonary embolism evaluation. MR axial fat–saturated T2-weighted image shows focal peripheral consolidation (white arrow) in the medial right lower lobe with central area of high T2 signal (dashed white arrow) surrounded by a hypointense rim (multiple short white arrows). Findings are consistent with consolidation with abscess formation, indicating focal abscess formation in the consolidation

nodules, pleural effusion, and lymphadenopathy. A study by Zeng et al. using the T2W propeller sequence to reduce respiratory motion found MRI to be promising tool for the subcategorization of tuberculous lesions which has treatment implications [48]. Parenchymal consolidation can be further characterized based on internal T2 signal intensity as representing caseous necrosis (low T2WI signal) as opposed to liquefactive necrosis (high T2WI signal).

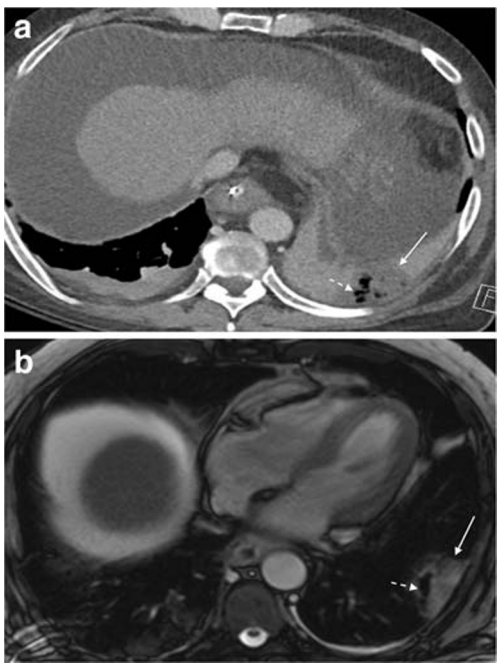

Fig. 7 Necrotizing pneumonia in a man presenting with sepsis. **a** Contrast-enhanced axial CT image shows left lower lobe consolidation with focal area of hypoenhancement (white arrow) containing interspersed gas (dashed white arrow). **b** MR axial TRUFISP after a few days showing mild improvement in left lower lobe consolidation (white arrow) with persistent gas seen as hypointense foci (dashed white arrow)

Differentiating tuberculoma from malignant nodules, without invasive tissue sampling, is often difficult as FDG-PET shows intense FDG uptake in both instances. However, these can be distinguished on MRI as tuberculoma demonstrate a "thin-rim enhancement" sign with minimal central enhancement [32].

Hamartoma

Hamartomas are benign neoplasms, originating from connective tissue of the bronchial wall, and are often discovered incidentally [32]. CT diagnosis relies on identification of intranodular fat interspersed with calcification with these typical imaging features present in only 50% of the cases. The remaining lesions are considered indeterminate due to the absence of calcification and/or macroscopic fat. MRI can be a problem-solving tool in these cases by demonstrating intralesional microscopic fat seen as drop-out of signal on out of phase images (Fig. 8). The hamartomas appear as well-circumscribed lesions with isointense signal on T1WI and high signal on T2WI [36].

Interstitial Lung Diseases

High-resolution CT is the imaging modality of choice for the diagnosis interstitial lung disease (ILD) complemented by lung biopsy. CT provides limited evaluation of acute inflammatory exacerbation and early fibrotic changes, both presenting as ground-glass opacities which can resolved by MRI to guide treatment (Fig. 9) [49, 50]. Inflammation appears as high signal on fluid sensitive T2WI with early post-contrast enhancement while lesions with predominant fibrosis demonstrate low signal on T2WI with late enhancement. Current research is investigating roles of collagen-targeted chelated MR agents and MRI of inhaled hyperpolarized gas for further functional imaging top assess ventilation and gas exchange which can further guide treatment management [51].

Sarcoidosis, often clumped under ILD spectrum, is a non-caseating granulomatous disease with perilymphatic nodularity and mediastinal lymphadenopathy. It is diagnosed at an early age, 25–40 years, which results in multiple CT studies over the course of life raising concern for cumulative radiation [50, 52, 53]. MRI can be used for routine follow-up and alleviate concerns regarding radiation. Additionally, tuberculosis can often mimic sarcoidosis on imaging which can be delineated on MRI by identifying necrosis in nodal tuberculosis [53]. Distinctive "dark lymph node sign" in sarcoidosis characterized by internal low intensity with peripheral rim of hyperintensity has been described in the literature and can further aid in problem solving [54].

MR Imaging of Pleural Disease

Benign Pleural Effusions

Pleural effusion results as an imbalanced equilibrium between the mechanisms for the production and absorption of pleural fluid. CT can reliably assess size and some complications of pleural effusions. MRI can be a problem-solving tool by assessing the subtle internal characteristics of the effusions bypassing needs for thoracentesis in special instances [55–57].

Simple effusion, consisting of simple fluid, appears as dependent crescentic low signal on T1WI and high signal on T2WI paralleling the CSF in spinal canal (Fig. 10). Exudative effusions present as high signal on both T1WI and T2WI [55, 56]. Fat content with a chylothorax can be

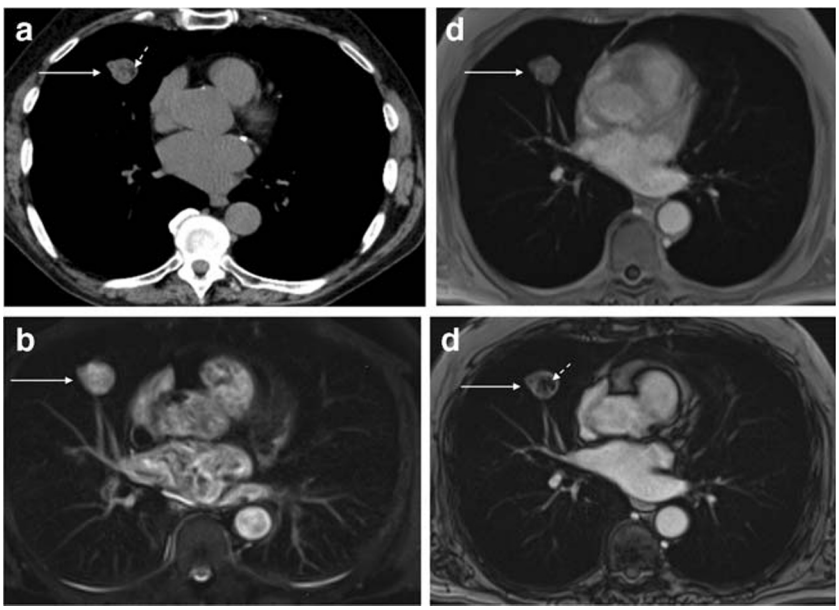

Fig. 8 Pulmonary hamartoma. **a** Non-contrast axial CT shows a well-defined right middle lobe nodule (white arrow) with internal fat attenuation (white dashed arrow). Subsequently performed MRI for characterization exhibits heterogenous hyperintense signal on **b** SSFP image. **c** In-phase and **d** out-phase imaging demonstrates signal dropout within the fat component (dashed white arrow) of the lesion (white arrow)

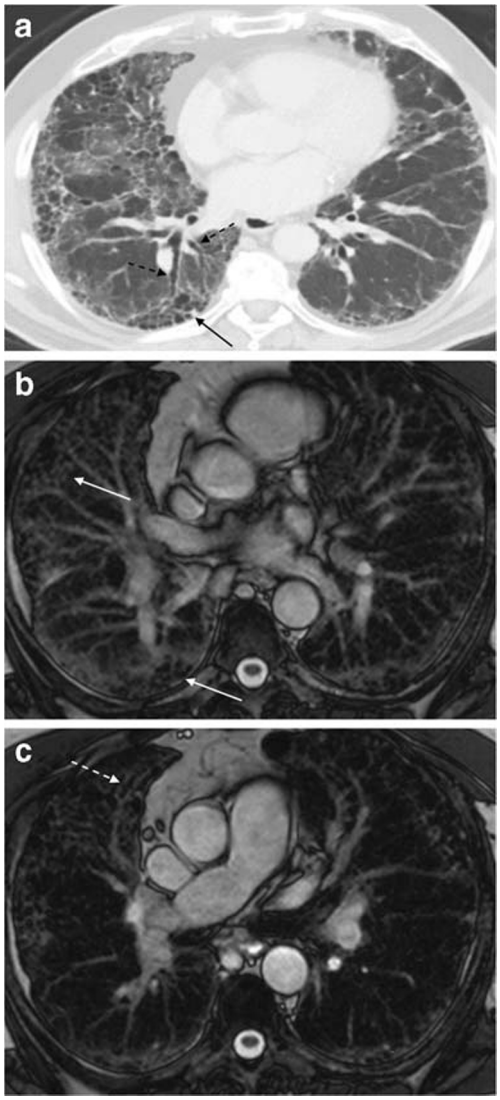

Fig. 9 Sixty-year-old man with usual interstitial pneumonia prior to lung transplant. **a** Non-contrast axial CT image demonstrates typical features of UIP, architectural distortion, traction bronchiectasis (black dashed arrows), and honeycombing (black arrow). **b**, **c** TRUFISP images show linear and nodular interstitial high T2 signal with honeycombing (white arrows) and traction bronchiectasis (dashed white arrow)

identified as high signal on T1WI. Areas of hemorrhage can also be identified as areas of low signal on T1WI and T2WI. A concentric ring sign, representing low signal of hemosiderin rim, has been described in hemothorax [55].

Malignant Pleural Effusions

Pleural metastases, most commonly from bronchogenic carcinoma, constitute the primary cause of malignant pleural thickening and effusions [55]. On CT, pleural thickening greater than 1 cm is considered highly suspicious for malignant process [55, 58]. A study by Hierholzer et al. comparing CT and MRI in evaluation of pleural nodules in 42 patients reported that the size criteria of greater than 1 cm are not accurate in

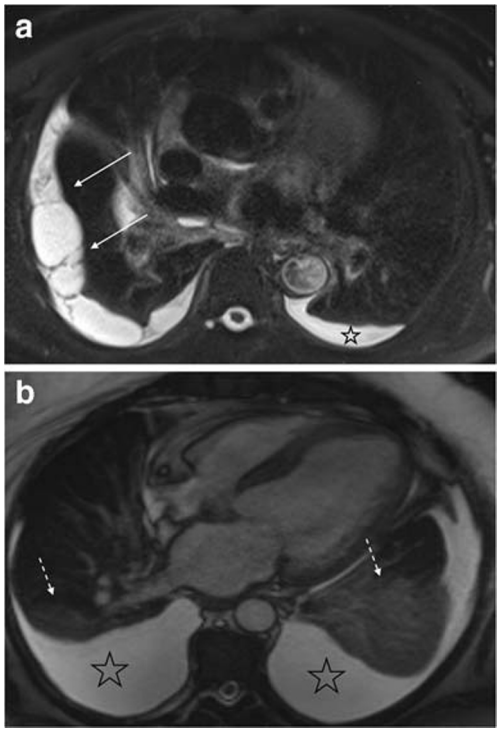

Fig. 10 **a** Axial fat–saturated T2-weighted image mildly complex right pleural effusion with loculations and internal T2 hypointense septations (white arrow) and simple left pleural effusion (star). **b** Axial steady-state free precision image, in a different patient, shows moderate-sized layering simple pleural effusions (stars) with associated adjacent compressive atelectasis which is uniformly mildly hyperintense (dashed white arrows)

distinguishing benign from pleural disease. However, MRI was superior to CT in differentiating these processes on basis of a combination of morphologic features and internal signal characteristics including high signal on T2WI in relation to intercostal muscles and enchantment of post-contrast images [59].

Early pleural nodular enhancement has also been reported to be a reliable marker of malignant involvement [60]. Malignant pleural disease on DWI demonstrates increase diffusion restriction, often a marker of high cellularity, and can be further used as an additional tool in thorough and non-invasive investigation of pleural disease [61, 62].

Thoracic Endometriosis

Chest is the most frequent extra abdominopelvic site of endometriosis, clinically presenting as cyclical chest pain as a response to presence of functional endometriotic tissue undergoing hormonal stimulation [63]. Pleural involvement by the disease can present as catamenial pneumothorax and catamenial hemothorax [64–66].

On MRI, the pleural lesions are seen as small T1 hyperintense lesions due to the presence of blood products and endometrial tissue from cyclical hemorrhage with associated hemopneumothorax or hydropneumothorax [64, 67]. The

pitfall in MRI is susceptibility related to air diaphragm interface which can be differentiated from true lesion by the linear shape parallel to the diaphragm and varying imaging appearances across different acquisitions and imaging planes [63, 64].

Malignant Mesothelioma

Malignant mesothelioma is the most common primary malignant tumor of the pleura related to asbestos exposure. On MRI, there is circumferential, rindlike, nodular pleural thickening appearing iso- to slightly hyperintense on T1WI and hyperintense on T2WI with post-contrast enhancement and diffusion restriction [55, 68].

MRI has an important role in mesothelioma staging due to the demonstration of extent of pleural involvement and local invasion into other organs or spaces. As per, International Mesothelioma Interest Group, locally advanced T3, which involves endothoracic fascia, mediastinal fat, non-transmural pericardial involvement or invasion of the chest wall soft tissue, can be surgically treated. Accurate pre-operative assessment is imperative as inoculation metastasis can develop after transthoracic drainage. Anatomical details such as extent of diseases into the recess often carry crucial consequences for radiation planning. T4 disease with extension into peritoneum or pericardium has dire prognosis with similar outcome as M1 disease [69].

Solitary Fibrous Tumor of the Pleura

A rare pleural tumor arises from the visceral pleura with a slight female predominance. They can be pedunculated and appear as low-to-intermediate signal intensity on T1W1 and T2WI due to low cellularity and presence of fibrous tissue with intense homogenous post-contrast enhancement (Fig. 11) [55, 69]. Focal areas of high signal on T2WI may be present due to necrosis or myxoid degeneration [55]. Superior soft tissue contrast of MRI allows for precise assessment of chest wall invasion which is a predictor of malignant potential. Real-time MR imaging demonstrates the movement of the mass separate from the chest wall motion in the absence of invasion.

Pleural Lipoma and Liposarcomas

Pleural lipomas are rare benign tumors with high signal on T1WI and moderate-to-high signal on T2WI, similar to subcutaneous fat with complete loss of signal on fat suppressed sequences. No internal soft tissue nodularity or post-contrast enhancement is seen. They have to be differentiated from liposarcomas which are large infiltrative mass with high signal of T2WI and low signal on T1W1 with heterogenous or nodular enhancement [55].

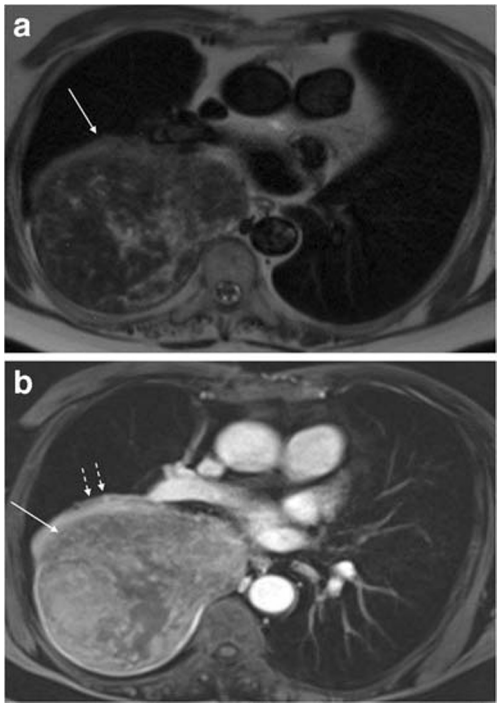

Fig. 11 Malignant solitary fibrous tumor of the pleura in a 80-year-old woman. **a** Axial T2-weighted image shows a large predominantly T2 hypointense extrapulmonary mass (white arrow) in the posterior right hemithorax exerting mass effect on the adjacent right lung and mediastinum. **b** Post-contrast T1-weighted image shows heterogenous enhancement (white arrow) with associated compressive atelectasis in posterior right lung (dashed white arrows)

MR Imaging of Vascular Abnormalities

Pulmonary vasculature evaluation can be performed with and without contrast. Results from PIOPED III study have shown a sensitivity of 55% and specificity of 99% for detection of acute pulmonary embolism (PE) in a technically adequate MR study. The sensitivity and specificity increased to 92% and 96% when coupled with MR venography. They concluded that MR pulmonary angiography should be performed at centers that have the expertise and in patients in whom standard tests are contraindicated [70–72].

Acute PE presents similarly on CT and MRI as central or complete intraluminal filling defects in pulmonary vasculature (Fig. 12). Failure of complete recanalization leads to chronic thromboembolic disease resulting in organized thrombi adherent to the walls which radiographically present as single linear bands and multiple bands resulting in web like structure and complex vascular occlusions or stenosis.

Complications such as pulmonary hypertension, right heart strain, and pulmonary infraction arising as a result of acute/chronic PE can be assessed using MRI [73]. Pulmonary infarcts present as peripheral wedge–shaped consolidation which tends to have high signal on T2WI and intermediate signal on T1WI during the immediate stages [74].

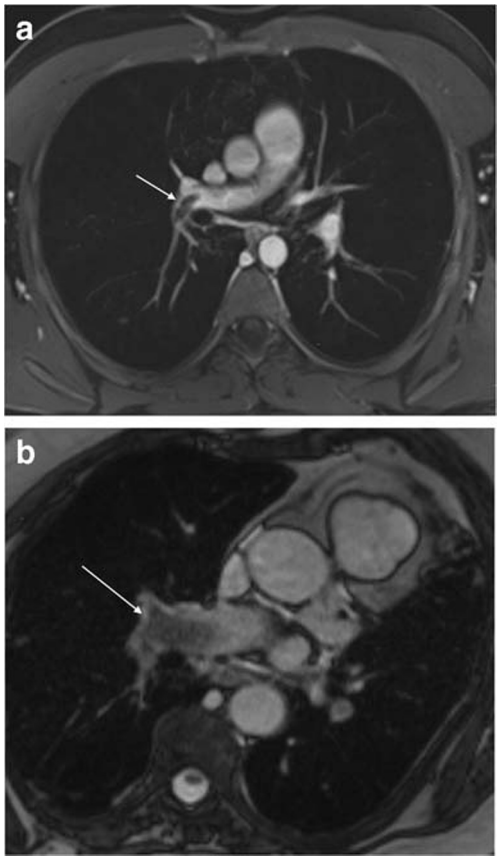

Fig. 12 Pulmonary embolism (PE) in two different patients. **a** Contrast-enhanced axial T1-weighted gradient echo image shows PE in the distal right and proximal right upper lobe pulmonary artery (white arrow). Non-contrast MRI (**b**) axial steady-state free precision image depicts right main pulmonary artery PE

MR Imaging of Airway Disorders

Cystic fibrosis, an autosomal recessive disorder, is characterized by abnormal mucus production. CT-based scoring systems have been developed to quantify disease severity with imaging findings such as bronchiectasis, peribronchial thickening, mucus plugging, air trapping, atelectasis, or consolidation. Regular monitoring of disease activity is important in assessing disease severity which needs to be balanced in young patients to control cumulative radiation. MRI of the lung is a viable option in these patients which is radiation free and provides both structural and functional information [75, 76].

MRI is particularly useful for assessing complications related to consolidation like necrosis (non-enhancing lung parenchyma), abscess formation (T2 hyperintense lesion with rim enhancement and diffusion restriction), and development of empyema. Perfusion imaging enables identification of perfusion defects related to hypoxic vasoconstriction in areas of decreased ventilation which is an early marker of disease progression and has prognostic implications. Recently, functional imaging with hyperpolarized xenon gas is evolving as a promising approach to evaluate regional lung function in cystic fibrosis. Results of pulmonary function testing in children are highly dependent on the subject's efforts and can be misleading which can be overcome with the use of functional MRI providing more consistent and reliable results [77].

Conclusion

Recent technical advents and increased accessibility have made MRI a viable clinical tool in a plethora of pulmonary pathology. We have discussed evolving role and value of MRI in some of these disease processes.

References

Papers of particular interest, published recently, have been highlighted as:
- • Of importance
- •• Of major importance

1. de Groot PM, Chung JH, Ackman JB, Berry MF, Carter BW, Colletti PM, et al. ACR Appropriateness Criteria® noninvasive clinical staging of primary lung cancer. J Am Coll Radiol. 2019;16(5):S184–95.
2. McComb BL, Ravenel JG, Steiner RM, Chung JH, Ackman JB, Carter B, et al. ACR Appropriateness Criteria® chronic dyspnea-noncardiovascular origin. J Am Coll Radiol. 2018;15(11):S291–301.
3. Harun HH, Karim MK, Abbas Z, Sabarudin A, Muniandy SC, Ng KH. Radiation doses and cancer risk from CT pulmonary angiography examinations.
4. Lahham A, ALMasri H, Kameel S. Estimation of female radiation doses and breast cancer risk from chest CT examinations. Radiat Prot Dosim. 2018;179(4):303–9.
5. Schwartz F, Stieltjes B, Szucs-Farkas Z, Euler A. Over-scanning in chest CT: comparison of practice among six hospitals and its impact on radiation dose. Eur J Radiol. 2018;102:49–54.
6. Dournes G, Macey J, Blanchard E, Berger P, Laurent F. MRI of the pulmonary parenchyma: towards clinical applicability? Rev Pneumol Clin. 2017;73(1):40–9.
7. Parwani P, Ramesh T, Akhter N, Iliescu C, Palaskas N, Kim P, et al. Differentiation of cardiac masses by cardiac magnetic resonance imaging. Curr Cardiovasc Imaging Rep. 2020;13(1):1.
8. Kapur S, Bhalla AS, Jana M. Pediatric chest MRI: a review. Indian J Pediatr. 2019;5:1–2.
9. Hirsch FW, Sorge I, Vogel-Claussen J, Roth C, Gräfe D, Päts A, et al. The current status and further prospects for lung magnetic resonance imaging in pediatric radiology. Pediatr Radiol. 2020;29:1–6.
10.• Raptis CA, Ludwig DR, Hammer MM, Luna A, Broncano J, Henry TS, et al. Building blocks for thoracic MRI: challenges, sequences, and protocol design. J Magn Reson Imaging. 2019;50(3):682–701 **The paper discusses the thoracic MRI protocol challenges and how to overcome them in clinical practice**.
11. Chang KJ, Kamel IR, Macura KJ, Bluemke DA. 3.0-T MR imaging of the abdomen: comparison with 1.5 T. Radiographics. 2008;28(7):1983–98.

12.•• Biederer J, Beer M, Hirsch W, et al. MRI of the lung (2/3). Why... when ... how? Insights Imaging. 2012, 3(4):355–71. https://doi.org/10.1007/s13244-011-0146-8 **One of the first papers detailing lung MRI protocol for clinical use based on expert consensus**.

13. Biederer J. General requirements of MRI of the lung and suggested standard protocol. In: Kauczor HU, Wielpütz MO, editors. MRI of the lung. Berlin Heidelberg: Springer; 2018.

14. Broncano J, Luna A, Caro P, Sanchez J, Vazquez J. Cardiac DWI: from basics to clinical applications. Eur Congress Radiol. 2018: C-2633. https://doi.org/10.1594/ecr2018/C-2633.

15. Winzer R, Hoberück S, Zöphel K, Kotzerke J, Brauer T, Hoffmann RT, et al. Diffusion-weighted MRI for initial staging in Hodgkins lymphoma: comparison with FDG PET. Eur J Radiol. 2020;123:108775.

16. Luna A, Sánchez-Gonzalez J, Caro P. Diffusion-weighted imaging of the chest. Magn Reson Imaging Clin N Am. 2011;19(1):69–94. https://doi.org/10.1016/j.mric.2010.09.006.

17.• Chen L, Zhang J, Bao J, et al. Meta-analysis of diffusion-weighted MRI in the differential diagnosis of lung lesions. J Magn Reson Imaging. 2013;37(6):1351–8. https://doi.org/10.1002/jmri.23939 **A meta-anlysis study evaluating role of DWI in differentiating benign from malignant lesions on chest MRI. This continues to be a highly investigated topic in MRI field to minimize need of invasive tissue sampling**.

18. Yumrutepe S, Turtay MG, Oguzturk H, Aytemur Z, Guven T, Turgut K, et al. Diffusion-weighted magnetic resonance imaging of thorax in diagnosis of pulmonary embolism. Med Sci. 2018;7:759–61.

19. Christodoulou AG, Shaw JL, Nguyen C, Yang Q, Xie Y, Wang N, et al. Magnetic resonance multitasking for motion-resolved quantitative cardiovascular imaging. Nature Biomed Eng. 2018;2(4):215–26.

20. Zeng G, Teng Y, Zhu J, Zhu D, Yang B, Hu L, et al. Clinical application of MRI-respiratory gating technology in the evaluation of children with obstructive sleep apnea hypopnea syndrome. Medicine. 2018;97(4).

21. Ebner L, Kammerman J, Driehuys B, Schiebler ML, Cadman RV, Fain SB. The role of hyperpolarized 129xenon in MR imaging of pulmonary function. Eur J Radiol. 2017;86(2017):343–52. https://doi.org/10.1016/j.ejrad.2016.09.015.

22. Muradyan I, Patz S. Hyperpolarized 129Xenon MRI of the lung. In: Kauczor HU, Wielpütz MO, editors. MRI of the lung. Berlin Heidelberg: Springer; 2018.

23. Nasim F, Ost DE. Management of the solitary pulmonary nodule. Curr Opin Pulm Med. 2019;25(4):344–53.

24. Robertson J, Nicholls S, Bardin P, Ptasznik R, Steinfort D, Miller A. Incidental pulmonary nodules are common on CT coronary angiogram and have a significant cost impact. Heart Lung Circulation. 2019;28(2):295–301.

25. MacMahon H, Naidich DP, Goo JM, Lee KS, Leung AN, Mayo JR, et al. Guidelines for management of incidental pulmonary nodules detected on CT images: from the Fleischner Society 2017. Radiology. 2017;284(1):228–43.

26. Donnelly EF, Kazerooni EA, Lee E, Henry TS, Boiselle PM, Crabtree TD, et al. ACR Appropriateness Criteria® lung cancer screening. J Am Coll Radiol. 2018;15(11):S341–6.

27.• Cieszanowski A, Lisowska A, Dabrowska M, et al. MR imaging of pulmonary nodules: detection rate and accuracy of size estimation in comparison to computed tomography. PLoS One. 2016;11(6):1–11. https://doi.org/10.1371/journal.pone.0156272 **An important study evaluating diagnostic accuracy of MRI in detection of pulmonary nodules of various sizes. Currently, pulmonary nodules greater than 4 mm on CT require follow-up. This study showed that these nodules can be readily identified on MRI**.

28. Sommer G, Tremper J, Koenigkam-Santos M, Delorme S, Becker N, Biederer J, et al. Lung nodule detection in a high-risk population: comparison of magnetic resonance imaging and low-dose computed tomography. Eur J Radiol. 2014;83(3):600–5. https://doi.org/10.1016/j.ejrad.2013.11.012.

29. Meier-Schroers M, Homsi R, Schild HH, Thomas D. Lung cancer screening with MRI: characterization of nodules with different non-enhanced MRI sequences. Acta Radiol. 2019;60(2):168–76. https://doi.org/10.1177/0284185118778870.

30. Wang X, Wan Q, Chen H, Li Y, Li X. Classification of pulmonary lesion based onmultiparametricMRI: utility of radiomics and comparison of machine learning methods. Eur Radiol. 2020;30:4595–4605. https://doi.org/10.1007/s00330-020-06768-y.

31. Ohno Y, Kauczor HU, Hatabu H, Seo JB, van Beek EJ, International Workshop for Pulmonary Functional Imaging (IWPFI). MRI for solitary pulmonary nodule and mass assessment: current state of the art. J Magn Reson Imaging. 2018;47(6):1437–58.

32. Ohno Y, Koyama H, Dinkel J. Lung cancer. In: Kauczor HU, Wielpütz MO, editors. MRI of the lung. Berlin Heidelberg: Springer; 2018.

33. Bruzzi JF, Komaki R, Walsh GL, Truong MT, Gladish GW, Munden RF, et al. Imaging of non-small cell lung cancer of the superior sulcus. RadioGraphics. 2008;28(2):561–72. https://doi.org/10.1148/rg.282075710.

34. Kratz JR, Woodard G, Jablons DM. Management of lung cancer invading the superior sulcus. Thorac Surg Clin. 2017;27(2):149–57.

35. Heelan RT, Demas BE, Caravelli JF, Martini N, Bains MS, McCormack PM, et al. Superior sulcus tumors: CT and MR imaging. Radiology. 1989;170(3):637–41.

36. Kurihara Y, Matsuoka S, Yamashiro T, Fujikawa A, Matsushita S, Yagihashi K, et al. MRI of pulmonary nodules. Am J Roentgenol. 2014;202(3):210–6. https://doi.org/10.2214/AJR.13.11618.

37. Kiryu T, Ohashi N, Matsui E, Hoshi H, Iwata H, Shimokawa K. Rounded atelectasis: delineation of enfolded visceral pleura by MRI. J Comput Assist Tomogr. 2002;26(1):37–8. https://doi.org/10.1097/00004728-200201000-00007.

38. Stathopoulos GT, Karamessini MT, Sotiriadi AE, Pastromas VG. Rounded atelectasis of the lung. Respir Med. 2005;99(5):615–23. https://doi.org/10.1016/j.rmed.2004.10.003.

39. Yang RM, Li L, Wei XH, Guo YM, Huang YH, Lai LS, et al. Differentiation of central lung cancer from atelectasis: comparison of diffusion-weighted MRI with PET/CT. PloS One. 2013 Apr 4;8(4):e60279. https://doi.org/10.1371/journal.pone.0060279.

40. Zhang X, Fu Z, Gong G, Wei H, Duan J, Chen Z, et al. Implementation of diffusion-weighted magnetic resonance imaging in target delineation of central lung cancer accompanied with atelectasis in precision radiotherapy. Oncol Lett. 2017;14(3):2677–82.

41. Jokerst C, Chung JH, Ackman JB, Carter B, Colletti PM, Crabtree TD, et al. ACR appropriateness criteria® acute respiratory illness in immunocompetent patients. J Am Coll Radiol. 2018;15(11):S240–51.

42. Lee C, Colletti PM, Chung JH, Ackman JB, Berry MF, Carter BW, et al. ACR Appropriateness Criteria® acute respiratory illness in Immunocompromised patients. J Am Coll Radiol. 2019;16(11):S331–9.

43. Liszewski MC, Görkem S, Sodhi KS, Lee EY. Lung magnetic resonance imaging for pneumonia in children. Pediatr Radiol. 2017;47(11):1420–30.

44. Marangu D, Gray D, Vanker A, Zampoli M. Exogenous lipoid pneumonia in children: a systematic review. Paediatr Respir Rev. 2019;33:45–51. https://doi.org/10.1016/j.prrv.2019.01.001.

45. Sehgal IS, Choudhary H, Dhooria S, Aggarwal AN, Bansal S, Garg M, et al. Prevalence of sensitization to Aspergillus flavus in patients

with allergic bronchopulmonary aspergillosis. Med Mycol. 2019;57(3):270–6.
46. Gao Y, Soubani A. Advances in the diagnosis and management of pulmonary aspergillosis. Adv Respiratory Med. 2019;87(6):231–43.
47. Sodhi KS, Gupta P, Shrivastav A, Saxena AK, Mathew JL, Singh M, et al. Evaluation of 3 T lung magnetic resonance imaging in children with allergic bronchopulmonary aspergillosis: pilot study. Eur J Radiol. 2019;111:88–92.
48. Zeng J, Liu Z, Shen G, Zhang Y, Li L, Wu Z, et al. MRI evaluation of pulmonary lesions and lung tissue changes induced by tuberculosis. Int J Infect Dis. 2019;82:138–46. https://doi.org/10.1016/j.ijid.2019.03.004.
49. Romei C, Turturici L, Tavanti L, Miedema J, Fiorini S, Marletta M, et al. The use of chest magnetic resonance imaging in interstitial lung disease: a systematic review. Eur Respir Rev. 2018;27(150):180062.
50. Lonzetti L, Zanon M, Pacini GS, Altmayer S, Martins de Oliveira D, Rubin AS, et al. Magnetic resonance imaging of interstitial lung diseases: a state-of-the-art review. Respir Med. 2019;155(April 2019):79–85. https://doi.org/10.1016/j.rmed.2019.07.006.
51. Weatherley ND, Eaden JA, Stewart NJ, Bartholmai BJ, Swift AJ, Bianchi SM, et al. Experimental and quantitative imaging techniques in interstitial lung disease. Thorax. 2019;74(6):611–9.
52. Arkema EV, Cozier YC. Epidemiology of sarcoidosis: current findings and future directions. Therapeutic Adv Chronic Dis. 2018;9(11):227–40.
53. Bhalla AS, Das A, Naranje P, Goyal A, Guleria R, Khilnani GC. Dilemma of diagnosing thoracic sarcoidosis in tuberculosis-endemic regions: an imaging-based approach. Part 2. Indian J Radiol Imaging. 2017;27(4):380.
54. Chung JH, Cox CW, Forssen AV, Biederer J, Puderbach M, Lynch DA. The dark lymph node sign on magnetic resonance imaging: a novel finding in patients with sarcoidosis. J Thorac Imaging. 2014;29(2):125–9.
55. Gill RR, Gerbaudo VH, Jacobson FL, Trotman-Dickenson B, Matsuoka S, Hunsaker A, et al. MR imaging of benign and malignant pleural disease. Magn Reson Imaging Clin N Am. 2008;16(2):319–39. https://doi.org/10.1016/j.mric.2008.03.004.
56. Yaddanapudi K. Benign loculated pleural effusion. InPET/MR imaging. Cham: Springer; 2018. p. 77–8.
57. de Fonseka D, Walker S, Maskell N, Edey A. S58 role of MRI in characterising equivocal pleural thickening on CT.
58. Kaul V, McCracken DJ, Rahman NM, Epelbaum O. Contemporary approach to the diagnosis of malignant pleural effusion. Ann Am Thoracic Soc. 2019;16(9):1099–106.
59. Hierholzer J, Luo L, Bittner RC, Stroszczynski C, Schoenfeld N, Dorow P, et al. MRI and CT in the differential diagnosis of pleural disease. Chest. 2000;118(3):604–9.
60. Tsim S, Humphreys CA, Cowell GW, Stobo DB, Noble C, Woodward R, et al. Early contrast enhancement: a novel magnetic resonance imaging biomarker of pleural malignancy. Lung Cancer. 2018;118:48–56.
61. Usuda K, Iwai S, Funasaki A, Sekimura A, Motono N, Matoba M, et al. Diffusion-weighted imaging can differentiate between malignant and benign pleural diseases. Cancers. 2019;11(6):811.
62. Keskin Z, Yeşildağ M, Alkan E, Kayhan A, Tolu L, Keskin S. Differentiation between transudative and exudative pleural effusions by diffusion weighted magnetic resonance imaging. Iran J Radiol. 2019;16(2):e78775. https://doi.org/10.5812/iranjradiol.78775.
63. Rezai S, Graves AG, Henderson CE. Thoracic endometriosis, a review. Obstet Gynecol Int J. 2019;10(5):342–6.
64. Montoriol PF, Da Ines D, Bourdel N, Garcier JM, Canis M. Re: thoracic endometriosis syndrome: CT and MRI features. Clin Radiol. 2014;69(5):549–50. https://doi.org/10.1016/j.crad.2014.01.023.
65. Rangunwala J, Sitta J, Vyas K, Roda M. Multimodality thoracoabdominal imaging findings in a rare case of thoracic endometriosis syndrome. Cureus. 2020;12(1):e6819. https://doi.org/10.7759/cureus.6819.
66. Maniglio P, Ricciardi E, Meli F, Vitale SG, Noventa M, Vitagliano A, et al. Catamenial pneumothorax caused by thoracic endometriosis. Radiol Case Rep. 2018;13(1):81–5.
67. Sanada T, Park J, Hagiwara M, Ikeda N, Nagai T, Matsubayashi J, et al. CT and MRI findings of bronchopulmonary endometriosis: a case presentation. Acta Radiol Open. 2018;7(10):2058460118801164.
68. Sinha S, Swift AJ, Kamil MA, et al. The role of imaging in malignant pleural mesothelioma: an update after the 2018 BTS guidelines. Clin Radiol. 2020. https://doi.org/10.1016/j.crad.2019.12.001.
69. Heussel CP, Wielputz MO, Kauczor HU. Disease of the pleura and the chest wall. In: Kauczor HU, Wielpütz MO, editors. MRI of the lung. Berlin Heidelberg: Springer; 2018.
70. Hosch W, Schlieter M, Ley S, Heye T, Kauczor HU, Libicher M. Detection of acute pulmonary embolism: feasibility of diagnostic accuracy of MRI using a stepwise protocol. Emerg Radiol. 2014;21(2):151–8. https://doi.org/10.1007/s10140-013-1176-y.
71. Marshall PS, Kerr KM, Auger WR. Chronic thromboembolic pulmonary hypertension. Clin Chest Med. 2013;34(4):779–97.
72. Aluja Jaramillo F, Gutierrez FR, Díaz Telli FG, Yevenes Aravena S, Javidan-Nejad C, Bhalla S. Approach to pulmonary hypertension: from CT to clinical diagnosis. Radiographics. 2018;38(2):357–73. https://doi.org/10.1148/rg.2018170046.
73. Nishiyama KH, Saboo SS, Tanabe Y, Jasinowodolinski D, Landay MJ, Kay FU. Chronic pulmonary embolism: diagnosis. Cardiovasc Diagnosis Therapy. 2018;8(3):253–71.
74. Yaddanapudi K. Pulmonary infarct. InPET/MR imaging. Cham: Springer; 2018. p. 71–2.
75. Scholz O, Denecke T, Böttcher J, Schwarz C, Mentzel HJ, Streitparth F, et al. MRI of cystic fibrosis lung manifestations: sequence evaluation and clinical outcome analysis. Clin Radiol. 2017;72(9):754–63. https://doi.org/10.1016/j.crad.2017.03.017.
76. Nagle SK, Puderbach M, Eichinger M, Altes TA. Magnetic resonance imaging of the lung: cystic fibrosis. In: Kauczor HU, Wielpütz MO, editors. MRI of the lung. Berlin Heidelberg: Springer; 2018.
77. Syrjala H, Broas M, Ohtonen P, Jartti A, Pääkkö E. Chest magnetic resonance imaging for pneumonia diagnosis in outpatients with lower respiratory tract infection. Eur Respir J. 2017;49(1):1601303.